Bias Properties of Extragalactic Distance Indicators XII: Bias Effects of Slope Differences and Intrinsic Dispersion on Tully-Fisher Distances to Galaxy Clusters with Application to the Virgo Cluster

Allan Sandage

The Observatories of the Carnegie Institution of Washington,
813 Santa Barbara Street, Pasadena, CA 91101-1292

What seems so simple is often highly complex in its dreadful detail:
Nilo Negge in the Book of Wisdom, 1619

ABSTRACT

The Teerikorpi incompleteness bias in the distance modulus of a galaxy cluster that is determined from incomplete data using the Tully-Fisher (TF) method is discussed differently than has been done in earlier papers of this series. A toy cluster is made with zero intrinsic TF dispersion but with slopes that differ between the calibrators and the cluster data, showing the bias caused by incorrect slopes. Intrinsic dispersion is added to the model and two strategies are used to analyze the data; first by binning the data by line width and then by apparent magnitude (the direct method), and second by binning by magnitude and then summing over all line widths (the inverse method). To illustrate these strategies, a composite cluster is made by combining the observations of Virgo A and B subclusters with those for the Ursa Major I and II clusters, corrected to the Virgo A distance. The cluster data are calibrated using Cepheid distances to 25 galaxies that have adequate TF properties. Different moduli calculated with varying completeness limits are displayed. The cluster modulus derived from the complete cluster sample gives $(m-M)^0 = 31.42 \pm 0.2$ (external) for Virgo A, 31.80 ± 0.16 for Virgo B, 31.26 ± 0.13 for UMa I, and 31.58 ± 0.17 for UMa II. Combining the Virgo A distance ($D = 19.2$ Mpc that has a range from 17.5 to 21.1 Mpc) with its expansion velocity of $1175 \pm 50\,\mathrm{km\,s^{-1}}$ as tied to the remote kinematic frame gives a Hubble constant of $61\,\mathrm{km\ s^{-1}\ Mpc^{-1}}$ with a range from 53 to 70.

Subject headings: Research — Tutorial — Galaxies — Data Analysis and Techniques

1. INTRODUCTION

The literature on the effect of bias in the measurement of extragalactic distances is extensive. Taken is a whole it seems comprehensive and exhaustive. Why then propose again an exposé of parts of the subject? The problem is not so simple in different situations, and new illustrations of the details can be useful.

A significant review, complete to 1996, is by Teerikorpi (1997). He treats many aspects of the problem beginning with the early insights of Kapteyn (1914), and then proceeds to the classical Malmquist (1920, 1922) and Scott (1957) effects.

The Malmquist calculation only concerns the bias integrated over a total sample. It does not show how the biased distance errors change as the truncation level is made fainter. Therefore, the classical Malmquist bias is not useful in correcting individual distances at various magnitude levels above the truncation level. For that, more complicated correction procedures mentioned below, are needed.

An equally complicated problem is to analyze the bias effects for individual galaxy distances using the Tully-Fisher line width (LW) method applied to field galaxies chosen in different ways, such as from magnitude-limited catalogs, or by imposing apparent diameter limits on 21-cm lists before measuring the radio line widths, or by restricting line widths at either the high and/or low LW limit, etc.

The literature on the use of the 21-cm line as a distance indicator began with the discovery of the correlation of LW with absolute magnitude by Roberts (1969), Gouguenheim (1969), and Bottinelli et al. (1971). The correlation was then developed as a distance indicator by Tully & Fisher (1977).

The bias properties of individual TF distances for field galaxies, chosen from magnitude-limited, or apparent diameter-limited samples, is clearly summarized by Teerikorpi in his important review. Correction procedures for bias can be made either by (1) the method of "normalized distances" (Teerikorpi 1984, 1990; Bottinelli et al. 1986; Theureau et al. 1997a,b) where a "plateau" is seen in an $M, (m - M)$ diagram that is calculated using TF distances and when all galaxies not on the plateau are discarded, or (2) corrected by a method such as the "triple entry" procedure (Sandage 1994a,b) or by the equivalent method of Spaenhauer diagrams (Sandage 1988a,b, 1994a,b, 1999; Federspiel, Sandage & Tammann 1994; Sandage, Tammann, & Federspiel 1995).

The problem of bias for *cluster* galaxy samples using the TF method would seem at first to be simpler than for TF field galaxy samples. Occasional early comments in the literature stated that bias problems for clusters do not exist because all members of the

sample are nearly at the same distance. This is incorrect. Bias still exists when a cluster luminosity function is sampled incompletely. Teerikorpi (1987, 1990) has called this the "cluster population incompleteness bias", of which there is now a significant literature.

A listing of the central papers on the incompleteness bias include those by Bottinelli et al. (1987), Bottinelli et al. (1988a,b), Kraan-Korteweg, Cameron, & Tammann (1988), Fouqué et al. (1990), Willick (1994), FST 94 (their Figs. 5, 6, & 8), STF 95 (their Figs. 2, 3, & 10), Giovanelli et al. (1997a,b), Teerikorpi et al. (1999), Masters et al. (2006) although we disagree with part of their analysis of the bias (Tammann, Sandage, & Reindl 2007), and by others cited therein. Why then is another paper on the cluster incompleteness bias useful, and what is the justification of this one?

Clarifications can be made on several points that include these. (1). Bias will exist with incomplete cluster sampling due to two separate effects, and it is useful to separate them.

(a). Applying an incorrect TF slope from the calibrating galaxies to the cluster sample is the principal reason for bias. Only when the adopted slope for the *calibrators* is the same as that of the *sample* can a slope bias be eliminated even if the cluster luminosity function is sampled "completely" in a certain way. This is true both for the "direct" and the "inverse" TF formulation, i.e. reversing what is the independent and dependent variables in the least squares regressions of LW on apparent magnitude.

The direct and inverse slopes will always be different in any correlation of two independent variables if there is intrinsic dispersion in the correlation (cf. Seares 1944; Feigelson & Babu 1992).

For the Tully-Fisher correlation it turns out to be crucial to use the correct slope in analyzing the data in either the direct or the inverse mode. However, there is the question of whether we should use the direct slope, the inverse slope, or something in between, sometimes called the compromise slope, in comparing the observed TF relation with any particular TF calibration.

(b). The second but related problem is the effect of the intrinsic dispersion of the TF correlation itself in the presence of incomplete sampling, even if a "correct" slope is used. The inverse formulation is free from bias in a sampling to different apparent magnitude limits (Schechter 1980; Tully 1988; Hendry & Simmons 1994; Ekholm & Teerikorpi 1997; Teerikorpi et al. 1999) if the LW distribution is complete (not truncated). However, this is true only if the inverse slope is used for *both* the calibrators and the cluster sample rather than the more usual practice of using the *direct* (or the compromise) slope that has been determined from the sample but which is then imposed upon the calibrators (§ 4 below) in using the inverse method for the sample. Rather, the inverse slope must be used for both

the calibrators and the sample.

(2). It has sometimes been written that the incompleteness bias would disappear if the scatter in the observed TF cluster LW-magnitude correlation (i.e. either an intrinsic TF dispersion or a back-to-front depth effect, or both) would be zero. This would only be true if the correct slope for the calibrators is used. However, such a slope is never known because of errors in the calibrator distances, giving a dispersion in the TF calibration solutions. This is the reason for the difference between the direct and inverse least squares solutions for the calibration. One of the purposes of this paper is to explore the effect of this dispersion both in the calibration and in the galaxy sample using a variety of TF slopes.

The effect of calibrator dispersion on the derived TF slope, especially in the direct mode, can be made particularly transparent using real calibration data from the HST Cepheid database for TF calibrating galaxies. We set out in § 4 a new Tully-Fisher calibration using our HST Cepheid distances (Saha et al. 2006). These are the basis of our 2006 distance scale with its determination of the Hubble constant (Sandage et al. 2006; Tammann et al. 2007).

(3). A different formulation of the TF bias problems can be made and can be compared with earlier discussions that may seem to have been unnecessarily opaque (eg. Sandage 1994b, Paper II). The present paper aims to clarify the TF bias problem, recasting the discussion in Paper II of this series by retracing the steps this author recently took in considering the subject again. The purposes here are fivefold.

(A). A simplistic toy (zero intrinsic dispersion) model is set out in § 2 showing what happens to the calculated distance moduli when an incorrect slope is used for the Tully-Fisher correlation for either the calibrators or the cluster data. A restriction to avoid a bias is stressed requiring that the depth of the magnitude sampling must be faint enough to be symmetrical about a "crossing point" in the $B_T^{0,i}$-LW correlation between the direct and the inverse regressions if the slope is incorrect.

(B). A more complicated toy model with intrinsic dispersion is discussed in § 3 with and without the correct slopes for the direct and inverse regressions.

(C). Real data are used in § 4 to make a mock (composite) cluster by combining observations for the spirals in the Virgo A and B cluster cores with similar data for the Ursa Major I and II spiral aggregates, corrected for the small distance differences.

(D). § 5 sets out a new calibration of the TF relation using our HST metallicity-corrected Cepheid distances (Saha et al. 2006; Sandage et al. 2006). This calibration using various slopes is applied to the composite cluster for both the direct and inverse regressions in § 6.

(E). The resulting distance to the Virgo Cluster A spiral core is set out in § 7. The Hub-

ble constant derived from this distance, using the cosmic expansion velocity of the cluster, freed from all local non-cosmological flows by tying to the distant cosmic kinematic frame, is set out there.

2. MODEL OF THE BIAS CAUSED BY INCORRECT TF SLOPES FOR THE CASE OF ZERO INTRINSIC TF DISPERSION; THE IMPORTANCE OF SYMMETRICAL SAMPLING OF THE MAGNITUDE INTERVAL

As said, even if the intrinsic TF dispersion (and/or an appreciable depth effect) would be zero, there would yet be a bias in a derived mean cluster distance if (1) an incorrect slope for the TF correlation is used, and (2) if the sampling is either incomplete at faint magnitudes or is non-symmetrical about the cross-over point of the direct and inverse slopes in the TF diagram. We illustrate these points using the simplistic model shown in Figure 1 that has a zero TF intrinsic dispersion.

The insert in Figure 1 shows a dispersionless TF correlation for an imaginary cluster that has a true slope of $dm/d\log w_{20} = -7$ and that is normalized at $B_T^{0,i} = 11.5$ for $\log w_{20} = \log W/\sin i = 2.50$. A calibration of the TF relation with a slope of -7 that gives $(m - M) = 31.5$ for the toy cluster is in the main body of the diagram, normalized at absolute magnitude -20 for $\log w_{20} = 2.5$. Two deviant slopes for the calibration are shown with slopes of -9 and -5. These cross the true slope at $M = -20$ and $\log w_{20} = 2.5$ by construction. These imitate (albeit with exaggeration) the inverse and direct least squares regressions for real calibration data (Figs. 5 and 6 in § 4.1). For real clusters the inverse correlation is always steeper than the direct. (The actual slopes for the 25 galaxy Cepheid calibration in § 6 are -6.161 for the direct regression and -8.475 for the inverse, from Table 7 later).

We can illustrate the bias on the calculated cluster moduli by using each of the calibration (incorrect) slopes of -9 and -5. Consider first the calibration slope of -9 applied to the toy cluster. This steep slope gives too bright an estimate of the absolute magnitude for all line widths larger than the cross-over point at $\log w_{20} = 2.5$, and hence the distance moduli are too large for all $\log w_{20} > 2.5$ and too small for line widths that are smaller than $\log w_{20} = 2.5$. The opposite is true for a slope of -5; galaxies with $\log w_{20}$ larger than 2.5 will be incorrectly calibrated too faint, giving smaller (incorrect) distances for $\log w_{20} > 2.5$ and too bright giving larger (incorrect) distances for $\log w_{20} < 2.5$.

In a complete sampling for LWs above and below $\log w_{20} = 2.5$, and if the number of

galaxies along the line in the insert diagram is constant, then the average distance modulus for the complete sample will be correct at $(m - M) = 31.5$. But this is true *only if the summing over all apparent magnitudes is carried out for magnitude limits that are symmetrical about the cross-over point* at $\log w_{20} = 2.5$ (or $B_T^{0,i} = 11.5$ in the toy model). Said differently, a correct mean modulus will only be obtained by summing over magnitudes that go to equal limits above and below 11.5, i.e. say from 10.0 to 13.0. If the magnitude boundaries are not symmetrical about this cross-over point (here at $B_T^{0,i} = 11.5$), or if there is a population gradient with magnitude, then the derived mean modulus will be incorrect. Of course, also if the summing over magnitude is incomplete (say only over the restricted interval of 10 to 12 mag), an incorrect mean modulus will be derived if the wrong slope is used.

This is the classical "population incompleteness" bias, but we see here that it is more complicated than simple incompleteness. It depends on slope errors and the necessity for symmetrical sampling above and below the cross-over point of the direct and inverse least squares solutions even if there is no gradient in galaxies numbers along the ridge line. This crucial point (see § 6) is illustrated in Table 1 for the dispersionless toy cluster that has been put at a true distance modulus of $(m - M) = 31.5$.

The first half of the table gives the calculated modulus at the fixed magnitudes in column (1) using arbitrary TF slopes that range from -9 to -5. Fixing all cross-over points of these lines to be $M = -20$ at $\log w_{20} = 2.5$ gives the equations of the assumed lines in the main body of the diagram as $M = -9 \log w_{20} + 2.5$ to $M = -5 \log w_{20} - 7.5$, etc., and $B_T^{0,i} = -7 \log w_{20} + 29.00$. All entries for $(m - M)$ at the stated apparent magnitudes in column (1) of Table 1 follow in an obvious way from these equations.

The calculated moduli for the slopes of -9 and -8 with apparent magnitudes brighter than 11.5 (the cross-over point) are larger than the true modulus of 31.5 and visa-versa for fainter magnitudes. The opposite trend exists for slopes of -6 and -5. These results are shown in Figure 2 (top). Of course, for the "true" slope of -7, all calculated moduli are 31.5 by construction.

Using the calculated moduli that are valid *at* the specified apparent magnitudes, we can sum the entries to obtain the average modulus value for all galaxies that are *brighter* than any particular limiting magnitude into the cluster luminosity function, shown in the bottom panel of Figure 2. These moduli are, of course, those that would be obtained in a real case by averaging the modulus values for all galaxies in the sample that is complete only to brighter magnitude limits. This is the incompleteness bias.

The effect of an incorrect slope on the bias using incomplete sampling is set out explicitly in the second half of Table 1, and shown in the bottom panel of Figure 2. The points to

note are these.

(A). For steeper slopes than the "true" slope (i.e. for -9 and -8), the derived mean distance moduli decrease as the sampling is done deeper into the cluster luminosity function. The bias effect from $B = 10$ to 13 is 0.4 mag in the modulus differences for the slope of -9 and 0.2 mag for the slope of -8.

(B). The opposite is true for the shallow slopes of -6 and -5.

(C). The correct modulus is obtained only by sampling to $B = 13$. This is three magnitudes into the cluster luminosity function.

(D). Sampling fainter than $B = 13$ gives incorrect modulus values (except for the -7 case using the "true" slope). This is the effect of "non-symmetrical" sampling about the cross-over point.

Of course, this toy model is too simplistic because there is no dispersion in the TF calibration nor in the TF correlation for the cluster galaxies.

3. A MODEL OF THE BIAS DUE TO AN INTRINSIC TF DISPERSION AND/OR INCORRECT SLOPES FOR THE TF RELATION

To understand the bias properties of the cluster TF data it is useful to analyze the LW-apparent magnitude data in two ways. The first is to bin the data into intervals of w_{20} and then, within each interval, to order the listings by apparent magnitude. The second is to bin the data by apparent magnitude and then to order by line width within each magnitude interval.

The first way is illustrated in Figure 3 where the intrinsic dispersion (plus any back-to-front variation) is shown by the dotted envelope lines placed symmetrically about the ridge line and where three line-width intervals are drawn for illustration. An arbitrary magnitude limit is put at $m = 11.5$, which is about 1.5 mag fainter than the brightest galaxy in the cluster in this example.

All galaxies in the line-width interval farthest to the right are brighter than the magnitude cut-off, whereas galaxies at smaller LWs to the left are progressively lost to the sample at smaller and smaller LWs. This causes the bias.

Consider first the unbiased LW interval to the right. Due to the dispersion, some galaxies are brighter than the central ridge line and some are fainter. If the position of the ridge line has been calculated by a least squares regression using magnitude residuals at fixed

w_{20}, i.e. in the "direct" solution, there will be equal numbers of galaxies above and below the calculated ridge line. This line is the most probable apparent magnitude at that w_{20}, although, because of the dispersion, no galaxy will have the ridge-line apparent magnitude unless, of course, it is on the ridge line.

Consider next how the data in this LW-interval are used to obtain a system of distance moduli using some absolute TF calibration such in Figure 8 later in § 5. The calibration will, itself, have a dispersion that will be a combination of the intrinsic dispersion due to the physics that governs the TF correlation and the measuring errors in the distances of the calibrating galaxies.

When the ridge-line calibration (i.e. the central line in Fig. 8 later) is applied to the ridge line of the *observed* cluster TF relation such as in Figure 3, a modulus value is obtained of each galaxy in that w_{20} interval. But, as said before, the calculated modulus of any given galaxy so obtained *is incorrect*, unless it is on the ridge line.

In detail, consider the unbiased $\log w_{20}$ interval from 2.70 to 2.75 for the right-hand strip in Figure 3. Suppose that all galaxies in the cluster are at the same distance (no back-to-front effect) and there are no errors of measurement either in w_{20} or magnitude. For this case, galaxies near the upper envelope line are those that are actually overluminous for their line width due to an intrinsic dispersion (i.e. from the physics) of the TF relation. Hence, applying the most probable calibration (which is fainter here than these particular galaxies) from the ridge-line calibrator relation to such *intrinsically* bright galaxies will give too small a calculated distance modulus for them, and visa-versa for galaxies that are actually underluminous (i.e. below the ridge line). Nevertheless, if the strip is filled symmetrically above and below the ridge line, and if the slope of that line has been determined by the "direct" least squares regression, then the mean modulus found by averaging the individual moduli in the strip (all of which are incorrect except for those on the strip) will be the correct modulus, to within statistics.

However, if the strip is not sampled completely, as in the second and third strips in Figure 3 where a magnitude cut truncates the distribution, the average of the individual moduli will be progressively in error at the smaller line widths as LW intervals move toward the left. The average of modulus values for galaxies above the magnitude limit line will then be too small by amounts that will decrease as the fraction of the accessible sample (the ratio to the complete sample) increases as the magnitude limit lines are moved fainter. *This is the incompleteness bias.*

Nevertheless, averaging over all line widths and to a sufficiently faint apparent magnitude will give the correct distance modulus if, of course, the strips are filled symmetrically

above and below the most probable ridge line.

This bias effect produces an error in the calculated *slope* determined from incomplete data in the direct regression. The error will be a function of the depth of penetration into the cluster luminosity function. This is obvious from Figure 3. The slope appropriate for the unbiased LW interval at the right ($\log w_{20}$ between 2.70 and 2.75) is the correct direct slope (except for statistics) that would be determined from the complete sample using the complete luminosity function. However, if we use only data brighter than any brighter magnitude cut, here put at 11.5 mag, the midpoint average magnitudes for the biased LW intervals (all to the left of the unbiased interval in Fig. 3) are all brighter than the true ridge line (unbiased) points shown by the three dots in Figure 3. Hence, the slopes that would be determined by calculation using only data brighter than any magnitude cut-off, *will all be too shallow*, approaching the correct slope only when the magnitude limit is so faint so as to include the complete sample.

Hence, because of the incompleteness bias, the calculated mean modulus using the direct slope should vary progressively with cut-off magnitude. This is the explanation of why in our earlier discussion (STF 95, Figs. 2, 3, 6, and 10) the calculated slope of the observed TF correlation in the direct formulation varies with cut-off magnitude. This effect on the slope will be demonstrated in § 4.1 (Fig. 7) using actual data.

The ideal schematic model of Figure 3 is still too simplistic because the effect of using an incorrect slope for the ridge line has been ignored. We mean by this that the (direct) slope shown in Figure 3, as it would have been derived from the complete sample, is assumed to be without error.

With this in mind, consider the inverse correlation where the calculated TF slope is independent of the depth sampled into the cluster luminosity function, in contrast to the direct slope calculated from incomplete data. The strategy of analysis for the inverse calculation is shown in Figure 4.

In Figure 4, as in Figure 3, the scatter of the cluster data at a given apparent magnitude is shown for a TF correlation that has intrinsic and/or back-to-front scatter. The inverse ridge line (marked I) is made to go through the midpoint of each shaded magnitude interval, because that is what the least squares regression gives by its procedure of using residuals in the LWs *at given magnitudes* rather than visa versa.

If the distribution of w_{20} within each magnitude interval is symmetrical about the ridge line, the average distance modulus of all the galaxies within each magnitude interval will be the true modulus to within statistics. This average at every magnitude interval will be bias free. However, as is evident in Figure 4, this will only be true if the inverse slope is used. It

will *not be true if the direct slope is used* with the inverse method.

Using either the I or the D ridge lines, and imposing in turn their slopes on the calibrator sample, gives individual modulus values for each galaxy in any of the individual strips in Figure 4. Again, as before, these individually are incorrect, except for galaxies precisely on the ridge line. Nevertheless, if the distribution of modulus values within each magnitude interval is symmetrical about the "I" ridge line, then the average of the individual modulus values within each magnitude interval will be the true value provided that the I slope *has been forced on the calibrators themselves*. Clearly, as seen from Figure 4, the same is not true using the direct slope. There are more galaxies to the small LW side of the TF distribution for magnitudes brighter than the cross-over point, and fewer galaxies to the left of the D line for fainter magnitudes than the crossover point. This produces the bias in the average modulus using the direct slope for all magnitude cut-offs brighter than the limit at $B = 14$. This is the cluster incompleteness bias in the direct formulation if the sampling is incomplete.

In the inverse method we need only average all the modulus data in a *given magnitude interval* to get the correct cluster modulus, in contrast to the direct method where we need to average over the whole of luminosity function, or we must apply the correction methods in the direct formulation derived either from the "normalized distance" method of the French workers (Teerikorpi 1997), or by the method of Spaenhauer diagrams (Sandage 1994a,b).

Figure 4 also shows the effect caused by an error in the adopted slope in the inverse method. This will cause a bias in the derived distance for the reason just described of using the direct slope when the inverse slope should be used.

Consider this effect of using the direct slope with the inverse method and summing the data only to a given apparent magnitude. Consider first all magnitude intervals that are brighter than the cross-over point at $m = 11.5$ and $\log w_{20} = 2.5$. An average modulus that is too small will be calculated at each of the bright magnitude intervals because there will be more galaxies to the left of the adopted "D" ridge line than to the right (i.e. giving moduli values that are too small compared with the ridge line average). The opposite will be true for all magnitude intervals that are fainter than $m = 11.5$ (seen also in the top part of Table 1 for a toy cluster with no dispersion). Only by summing the total data over all magnitude intervals can the correct true modulus be obtained. However, as in Figure 1 and Table 1, the sum over all magnitudes in a complete sample must be made no fainter than the magnitude level that is *symmetrical* about the cross-over point, showing again the need to adopt a symmetrical magnitude limit about the cross-over point in both the direct and inverse solutions.

Hence, on both accounts of the effect of (1) incomplete sampling using the direct TF

slope as in Figure 3 and then summing over all magnitudes (usually such completeness is not available), or (2) of summing over LW to given magnitude limits (Fig. 4 for the inverse method), the conclusion is that the true inverse slope must be used to avoid both (a) the error in the adopted slope and (b) the incomplete sampling effects. These conclusions will be demonstrated in § 6 using real data for a composite (artificial) cluster.

4. A COMPOSITE CLUSTER MADE TO ILLUSTRATE THE INCOMPLETENESS BIAS

4.1. Construction of the Composite Catalog

To demonstrate the points made in the last two sections it is useful to analyze real LW and magnitude data for a galaxy cluster. Only a few catalogs exist that are complete enough for real clusters to be useful for such a demonstration. The most complete are for the Virgo A and B subclusters and for the Ursa Major "cluster", early called the Ursa Major Cloud by Hubble and identified as such by Humason et al. (1956) in the Mount Wilson redshift list.

However, the number of spirals that are suitable for a TF analysis (inclinations greater than 30° and adequate photometry to derive fully corrected apparent magnitudes) in these three aggregates is so small that small-number statistics can mask the bias effects we are seeking. To increase the size of the sample we have created a composite cluster by combining the data for the Virgo A and B subclusters with those for the Ursa Major cloud to form a single catalog. Corrections have been made to the apparent magnitudes of the galaxies in the Virgo B cluster and the Ursa Major Cloud to compensate for the small differences in the distances of each aggregate relative to Virgo A.

The data for the Virgo subclusters are taken from the listings by Federspiel, Tammann, & Sandage (1998) in their Table 3. Membership for Virgo A and B are based on the Virgo Cluster Catalog of Binggeli, Sandage, & Tammann (1985) as reanalyzed for cluster members by Binggeli, Popescu, & Tammann (1993). Only galaxies with inclination greater than 30°, and only those assigned either to subclusters A and B are used. There are 43 galaxies in Virgo A and 16 in Virgo B in the composite catalog.

The Ursa Major Cloud has been studied in the past by Sersic (1960), de Vaucouleurs (1975, especially his Figs. 8 & 9) in his review of groups, Tully & Fisher (1987), Pierce & Tully (1988), Verheijen (1997, his Fig. 7 in chapter 4 of his thesis), Tully et al. (1996), Peletier & Willner (1993), Federspiel (1999), and undoubtedly others.

We use here the cluster membership of Federspiel from his Table 3.2 for the spirals that

are suitable for the TF method where he lists the necessary $B_T^{0,i}$, line width, and v_{220} radial velocity data (to test membership). Federspiel's membership criteria, similar to those of Verheijen and of Pierce & Tully, are (a) heliocentric redshift interval from 700 to 1500 km s^{-1}, and (b) angular distance within 7.5° of RA(1950)= $11^{\rm h}54^{\rm m}$, Dec(1950)= +49.5°.

The radial velocity distribution in v_{220}, corrected for Virgo infall by the model of Kraan-Korteweg (1986), shows a bimodal character with means at 1060 ± 29 km s^{-1} and 1485 ± 38 km s^{-1}, indicating an appreciable depth effect along the filament connecting the cloud with the Virgo complex that is shown so remarkably in Figure 6 of Klypin et al. (2003). We treat separately the two distributions, assigning galaxies with $v_{220} < 1250$ km s^{-1} to be members of an Ursa Major I aggregate, and those with $v_{220} > 1250$ km s^{-1} as members of Ursa Major II. There are 18 spirals suitable for the TF method in UMa I and 15 in UMa II.

Hence, there are 92 galaxies in the artificial composite cluster (43, 16, 18, and 15) from Virgo A, Virgo B, and UMa I and UMa II.

The $B_T^{0,i}$ magnitudes used here, corrected to a "total" magnitude, are within a few hundredths of a magnitude of the RC3 (de Vaucouleurs et al. 1991) system. (Slight differences at the few hundredths mag level exist because no K redshift corrections were applied here, differing from the RC3, and some updating was made). The LW data for the four aggregates are on the homogeneous line-width system used by FTS 98, taken from the Lyon-Meudon Extragalactic Data Base (the LEDA). These LWs average 0.033 ± 0.002 dex smaller than the LWs that are calculated from the RC3 with the RC3 inclinations calculated from the $\log R_{25}$ values listed there.

Small magnitude corrections between the four groups are needed to reduce all data to the distance of Virgo A. These were determined by comparing the zero points of the least squares TF correlations of Virgo A with those of Virgo B and UMa I & II. To calculate these corrections, the Virgo A TF slope is imposed on Virgo B and UMa I & II. These gave zero point magnitude differences such that the $B_T^{0,i}$ magnitudes for Virgo B are made brighter than the FTS 98 listings by 0.38 ± 0.16 mag (Virgo B is more distant). The correction for UMa I (the smaller velocity aggregate) is 0.16 ± 0.13 mag made fainter than the magnitudes listed by Federspiel (1999) (UMa I is closer than Virgo A), and the Federspiel magnitudes for UMa II (the larger velocity aggregate) were made brighter by 0.16 ± 0.17 mag (UMa II is more distant than Virgo A) so as to put the magnitudes on the distance system as Virgo A.

Using these magnitude corrections we have made an artificial cluster catalogue from which the TF correlation of $\log w_{20}$ with the $B_T^{0,i}$ magnitudes can be made. The result is in Figure 5 where all 92 galaxies of the artificial composite cluster are shown. A more select subsample of 84 galaxies is shown in Figure 6 where a magnitude cut is made at $B_T^{0,i} = 14.0$,

eliminating the eight faintest galaxies.

The slopes of the direct and the inverse least squares regressions with the cluster data are shown in parentheses in the diagrams. The equations of the regression lines are:

$$B_T^{0,i}(\mathrm{RC3}) = -6.622 \log w_{20}\ (\mathrm{LEDA}) + 28.195 \pm 0.103, \tag{1}$$

for the direct regression using all 92 galaxies in Figure 5, and

$$B_T^{0,i}(\mathrm{RC3}) = -8.032 \log w_{20}\ (\mathrm{LEDA}) + 31.598 \pm 0.114 \tag{2}$$

for the inverse correlation for the same sample.

The equations for the more restricted 84 galaxy sample (cut at $B_T^{0,i} = 14.0$) are:

$$B_T^{0,i}(\mathrm{RC3}) = -5.936 \log w_{20}\ (\mathrm{LEDA}) + 26.453, \tag{3}$$

for the direct regression, and

$$B_T^{0,i}(\mathrm{RC3}) = -7.547 \log w_{20}\ (\mathrm{LEDA}) + 30.391. \tag{4}$$

4.2. The Sensitivity of the TF Slope with Sampling Depth into the Cluster Luminosity Function

The data for the artificial cluster have been binned by apparent magnitude, enabling a study of the effect on the biased slope of the Tully-Fisher correlation due to incomplete sampling. Least squares solutions have been made from the composite cluster data as the magnitude cut is put progressively fainter. The results are listed in Table 2 in columns (2-6) for the total sample of 92 galaxies to the limit of $B = 15$, and for the restricted sample of 78 galaxies in columns (7-9) to be discussed later in § 6.

Column (1) shows the magnitude cut into the luminosity function of the composite cluster. The number of galaxies to each truncated limit is in column (2). The slope and zero point for the direct regression (residuals taken in magnitude at a fixed LW as in $m = a \log w + b$), are in columns (3) and (4). The slope and zero points of the inverse correlation, as in $log w_{20} = cB_T^{0,i} + d$, are in columns (5) and (6). The slopes and zero points for the complete sample of $n = 92$ for $B > 15$ (the last row) are, of course, the same as in equations (1) and (2). Columns (8) and (9) show the calculated least squares direct and inverse slopes for the restricted sample ($n = 78$) to the listed cut-off magnitudes. The number of galaxies to that magnitude limit is in column (7).

Figure 7 shows the data in Table 2 where the progressive increase of slope for the direct correlation, consistent with Figs. 2, 3, 6, and 10 of STF 95, is evident. The top panel shows the increase of slope with increasing faintness for the direct formulation using the complete sample of 92 galaxies (col. 3 of Table 2). Less clear but consistent within statistics, is the lack of a correlation of slope with faintness for the inverse correlation. The bottom panel shows the same effect more clearly for the restricted sample of 78 galaxies from columns (8) and (9) of Table 2.

The expectation from § 3 (eg. from Fig. 3) is that there should be a progressive change of slope as the cluster is sampled more deeply in magnitude using the DIRECT regression (residuals in magnitude at given LW), whereas no systematic variation should be present in the INVERSE solution (residuals in LW at given magnitudes). Figure 7 shows the slope effect in the DIRECT (dots) formulation. It is consistent with Figures 2, 3, 6, and 10 of STF 95.

The situation is less clear in support of the prediction of no-slope variation for the inverse regression (open circles) because of the dip between 12 and 13 mag and the increase at fainter magnitudes. However, inspection of the distribution of galaxies within the envelope lines in Figures 5 and 6 shows the reason is the statistical noise caused by fluctuations in the small number statistics of the actual data, and the evident non-uniform filling of the vertical and horizontal bins in Figures 3 and 4, seen by inspection of Figures 5 and 6 here, and especially Figure 7 of FTS 98. In Figures 5 and 6 for the magnitude interval from $B = 12$ to 13 there are more galaxies to the left of the ridge lines than to the right, and conversely, from magnitude 13 to 14 the opposite is true. This causes the entries in the later Tables 5 and 6, used to construct a magnitude-modulus diagram similar to Figure 2, to show this statistical noise as curvature from $B = 12$ to 14, reducing the ideal symmetry of Figure 2 for the toy cluster to the noisy reality of the real data for the composite cluster. We shall encounter the problem again in § 6 where the data for the composite cluster using various TF slopes resembles Figure 2. This statistical noise between $B = 12$ to 14 degrades the predictions of the ideal noiseless toy cluster of Figures 1 and 2.

To this point we have not needed an absolute magnitude calibration of Figures 5 and 6 to study the bias problem. In particular we have not needed a calibration to obtain Table 2 and Figures 7, but to carry the argument further we now do.

5. A NEW TF CALIBRATION USING HST CEPHEID DISTANCES FOR 25 GALAXIES

Equations (1-4) and Figures 5 and 6 are only useful for determining distance moduli if a calibration of the TF regression in absolute magnitude is available from independent data. We use here a new calibration based on 25 galaxies in which Cepheids have been measured, the majority of have been observed with the HST space telescope. The new data are set out in Table 3.

Column (1) lists the galaxy name. The type and luminosity class are in column (2) from the listings in A Revised Shapley Ames Catalog of Bright Galaxies (Sandage & Tammann 1981, 1987). Column (3) is the adopted distance modulus from Saha et al. (2006, Table 8) based on period-dependent metallicity corrections required by the non-unique Cepheid period-luminosity relations that vary from galaxy-to-galaxy (Tammann, Sandage, & Reindl 2003; Sandage, Tammann, & Reindl 2004; Kanbur & Ngeow 2004; Ngeow & Kanbur 2005; Ngeow et al. 2005). These modulus values define our 2006 distance scale based on type Ia supernovae and HST Cepheids (Saha et al. 2006; Sandage et al. 2006). (The listed modulus for NGC 4258 corrects the value listed in Table 8 of Saha which was a computational error).

Column (4) is the fully corrected apparent magnitude on the scale of FTS 98 which is close to that in the RC3. Column (5) is the $M^{0,i}_{B(T)}$ absolute magnitude which is column (4) minus column (3). The log line width at the 20% level and corrected for inclination is in column (6) on the Lyon-Meudon Extragalactic Data Base (LEDA) as set out in FTS 98. Where no data exist in FTS 98 we use the RC3 LW data made smaller by 0.033 dex.

The difference in the distance moduli in column (3) with 16 galaxies in common with FTS 98 is 0.05 ± 0.03 mag with the distances in Table 3 being larger.

Comparisons of the distance scale here with that of Freedman et al. (2001, Cols 2 and 5 of their Table 3) are these. The difference between Table 3 here and Table 3, column (2) of Freedman et al. (their old scale) is 0.09 ± 0.04 mag from 25 overlaps. Our distances are larger. The difference using the new scale of Freedman et al. (their Table 3, col. 5) is 0.23 ± 0.04 mag, again our distances are larger.

Comparing the larger sample of all Cepheids (not just those that make up the TF calibration) that are in common between our scale and Freedman shows $(m - M) = 0.11 \pm 0.03$ mag for Freedman's old scale (col. 2 of their Table 3) from 30 overlaps. Their new scale (col. 5 of their Table 3) compared with ours shows $(m - M) = 0.25 \pm 0.04$ mag from 30 galaxies in common. Again our scale is longer.

The reason for the difference is that we account for the different slopes and zero points

of the Cepheid P-L relations from galaxy-to-galaxy according to metallicity corrections that are period dependent (Saha et al. 2006). The P-L slopes differ depending on metallicity (Fig. 5 and Table 4 of Tammann et al. 2007), whereas those of Freedman et al. do not. For their new scale (column 5 of their Table 3), they adopt the shallow LMC P-L slope, not the steeper slope for the Galactic Cepheids which we have argued elsewhere (Tammann et al. 2007) that they should have used.

The data from Table 3 are plotted in Figure 8 where the direct and inverse least squares regressions are shown with their slopes in parentheses. These slopes differ from the regressions for the composite cluster in Figures 5 and 6. They *must not* be used in analyzing the cluster data. Rather, the cluster slope must be imposed on the calibrator data (§ 6) to obtain the calibrator zero point that is appropriate for the cluster data. This requirement is fundamental to avoid bias errors due to slope differences. This crucial point concerning the correct slope to use has sometimes been overlooked in the earlier literature on the TF method.

6. BIAS IN THE DERIVED DISTANCE MODULUS DUE TO INCOMPLETE SAMPLING IN THE ARTIFICIAL CLUSTER USING BOTH THE DIRECT AND THE INVERSE TULLY-FISHER REGRESSIONS

Individual distance moduli have been calculated for all galaxies ($n = 92$) in the artificial cluster using both the direct and inverse slopes. The calibration using the Cepheid data in Table 3 has been zero pointed by imposing the cluster slopes of -6.622 and -8.032 from equations (1) and (2) on the Cepheid calibrators. These give the Cepheid ridge-line calibrations of

$$M^{0,i}_{B(T)}(\mathrm{FTS}) = -6.622 \log w_{20}\ (\mathrm{LEDA}) - 3.369 \pm 0.103 \tag{5}$$

for the direct regression, and

$$M^{0,i}_{B(T)}(\mathrm{FTS}) = -8.032 \log w_{20}\ (\mathrm{LEDA}) + 0.239 \pm 0.114 \tag{6}$$

for the inverse.

The individual (most probable, but all incorrect because of the dispersion except for galaxies on the ridge lines) moduli follow in an obvious way by combining these Cepheid ridge-line calibrations with the individual apparent magnitude and LW data for each galaxy in the cluster.

Following Figure 3, the data were first separated into $\log w_{20}$ intervals in steps of 0.1 dex. They were then binned in apparent magnitude intervals of 0.5 mag and averaged.

The average modulus in each w_{20} interval and each magnitude bin are shown in Table 4. The number of galaxies that make up each average is in parentheses.

The bias properties discussed in § 3 can now be illustrated using Table 4 rather than by relying on hypothetical models. These properties and their consequences can most easily be understood by using Table 4 and referring to Figures 3 and 4 for the two binning strategies. There are three principal points.

(1). Table 4 shows that within any given LW interval (columns 2-8) the average moduli show a systematic variation as the apparent cut-off magnitude is made fainter. This is expected from the discussion of Figure 3 in § 3. The variation is due to this.

All galaxies in Figure 3 that are brighter than the ridge line magnitude at any LW have calculated moduli that are *smaller* than the ridge-line (the true) value and visa versa for those below the ridge line. Figures 9a and 9b show the trend of the individual moduli for both the direct and inverse slopes in the six LW intervals that range from 2.6-2.7 to 2.1-2.2.

The expectation (§ 3) that becomes manifest in Table 4A is that the average over all magnitudes (i.e. summed vertically in each column of Table 4A) should not vary systematically *with LW* to within statistics using the DIRECT slope because the DIRECT ridge line threads strictly down the middle of each vertical column of Figure 3 by its least squares construction. This expectation is realized to within statistics by the averages set out at the bottom of Table 4A for each LW interval.

In contrast, using the INVERSE slope, the averages over all magnitudes *at given LW*, as analyzed via Figure 4, is expected to vary systematically with LW, meaning that the averages at the bottom of Table 4B should show a strong systematic variation with LW because the INVERSE ridge line, not shown in Figure 3, *does not* thread the middle of the vertical LW columns. This expectation is well seen in the strong variation, outside the statistical noise, of the average moduli shown in Figure 9b marked by the arrows, and seen in the bottom row of Table 4B.

(2). However, rather than first binning by LW and then magnitude, the more realistic analysis, and the one always made in practice, is to work with averages made by summing over all line widths at various magnitude limits. The strategy is illustrated in Figure 4 using progressively fainter magnitude cut-offs. Here, we are interested in the bias properties of Tables 4A and B by summing over *all line widths* to various cut-off magnitude limits. The method using Tables 4A and B is to sum horizontally (over all LW) in each magnitude

interval, and than sum over all magnitude intervals up to a given magnitude cut-off.

The results are given in Table 5 which is divided using the direct slope of −6.622 in the top half and the inverse slope of −8.032 in the bottom half. Column (1) shows the magnitude intervals used in Table 4. Column (2) is the number of galaxies used in the averages. Column (3) gives the average modulus for all galaxies summed over all LWs in this magnitude interval. These are calculated by summing the Table 4 entries horizontally in each magnitude interval. Column (4) is the rms variation of these averages. Columns (5-8) give the average moduli calculated by summing the data in column (2) *up to* the magnitude cut-off listed in column (5). The number of galaxies making up this sum is in column (6). This is the accumulated number of galaxies by summing column (2). The mean modulus of the accumulated sums is in column (7). The rms of these averages is in column (8).

(3). The expectation from § 3 is that the inverse slope must be used in summing horizontally in Table 4 as in Figure 4 to avoid bias. If so, there should be no systematic bias increase in the derived distance modulus based on the inverse slope as the grasp into the cluster luminosity function is deepened. However, this should not be true in the direct formulation where the derived average modulus is expected to increase with fainter magnitude cut-offs.

These expectations are verified in Figure 10 where the data from Table 5 are plotted. Open circles are for the magnitude intervals in column (1). Crosses are for the accumulated data listed in column (7). The expectations from the discussion in § 3 are fulfilled to within statistics in the two panels of Figure 10.

6.1. Effect of Using an Incorrect Slope for the TF Correlation

Table 5 and Figure 10 are based on the formal least squares slopes for the TF data for the composite cluster for both the direct and inverse calculations. It is of interest to gauge the effect of systematic errors in these slopes by arbitrarily varying them over a wider range than given by the regressions on the actual.

We have chosen TF slopes of −9, −7, −6, and −5 to add to the results in Table 5. These cover the same range of slopes as in the toy cluster of Figures 1 and 2. The calculation was made by first redoing the Cepheid zero point calibration by imposing each of the assumed slopes on the Cepheid data in Table 3. These M, $\log w_{20}$ zero point calibrations were then applied to each of the 92 galaxies giving individual $(m - M)$ modulus values for each cluster galaxy. These were then binned by apparent magnitude and summed over all LW for the galaxies brighter than a given apparent magnitude to produce a mean modulus for that

TF slope and apparent magnitude cut-off. The results are listed in Table 6, which can be combined with those in Table 5 for the slopes of −6.622 and −8.032 and Table 8 later for slopes of −6.346 and −7.519.

Column (1) is the magnitude depth that is sampled into the cluster luminosity function. The number of galaxies making up the averages is in column (2). The average moduli to the cut-off magnitude are in columns (3), (5), (7), and (9). The rms of these listed moduli are in columns (4), (6), (8), and (10).

Table 6 for the slopes of −9 to −5 combined with Table 5 for the data with the slopes of −6.622 and −8.032 show many of the general features of Figure 2 and Table 1.

As expected, the systematic run of moduli with apparent magnitude exists for all slopes that differ from the inverse slope of −8.032. For slopes steeper than this (−9 in Table 6) the sign of the bias is that smaller moduli are calculated as the magnitude grasp into the cluster is increased. The opposite sign of the bias is evident (larger moduli for deeper cluster penetration) is seen for slopes flatter than −8.032.

However, the detailed results, seen by plotting the data in Tables 5 and 6 (not shown), are not as clear as in the noiseless model of Table 1 and Figure 2. From Figure 2 (bottom) we expect that the null magnitude (where all modulus values converge) should be at $B = 13$, which is about 3 mag fainter than the brightest galaxy. However, the results for the composite cluster using real data show that the null magnitude is near $B = 12$ from Table 6 and between $B = 12$ and 12.5 from Table 5. As explained in § 4.2, the small-number statistical noise in the distribution of points between $B = 12$ and 14 is the probable cause of this difference. This shows the limitation on the accuracy of the TF method due to random noisiness within the dispersion when only a small number of cluster galaxies are available. Of course, the situation is improved using I magnitudes where the dispersion is smaller but the slope of the TF regression is near 10, adding additional uncertainties.

7. DISTANCE TO THE VIRGO A SPIRAL CLUSTER CORE LEADING TO THE GLOBAL VALUE OF THE HUBBLE CONSTANT

From the results concerning bias set out in the previous sections, how then do we use them to find the most probable distance modulus of the composite cluster?

From analysis of the properties of the bias given above and from the results of Figures 7, 10, and 11 it might seem best to use only the moduli based on the inverse analysis because, given large enough samples, there is no bias. However, there are two reasons we have not

done this.

(1). The rms variation of the modulus summed to various magnitude limits, listed in Table 5 and later in Tables 7 and 8 in § 7.1, is always smaller for the direct formulation than for the inverse in a ratio of about 1.2 (eg. 0.576 to 0.488 from the penultimate rows of Table 5). Hence, the direct moduli have greater weight than the inverse by a factor of about 1.4.

(2). There are always differences in the final average moduli between the direct and inverse calculations that are independent of the bias problems. The cause is different Cepheid calibrations between the direct or inverse calculations. This is because a given galaxy will be assigned different absolute magnitudes depending on the two different calibrations of zero point. When the sums over all galaxies are taken, these will not average out because the direct and inverse magnitudes have different weights. The experience here (Table 5 summed to $B = 14$, Table 7 col. 7 in § 7.1, and Table 8 also later in § 7.1), the mean modulus taken over all cluster galaxies is always larger for the direct calculation than for the inverse. The modulus difference between the direct and inverse is always smaller when their slope difference is smaller, seen from the second half of Table 7.

In view of these two reasons, which regression should we use to obtain the best distance modulus? We have decided not to decide between them but to reduce the data with both, avoiding the bias corrections for the direct method by summing to $B = 14$, a magnitude that is symmetrical brighter and fainter than the cross-over point of the direct and inverse regressions.

7.1. The Cepheid and Cluster Zero Point Calibrations Using Various TF Slopes

For each adopted TF slope for the cluster sample we must determine new zero points for the Cepheid calibration based on Table 2 of § 2 by forcing the adopted slope on the calibrators and calculating the resulting intercept for the calibration equation. (As said before, this point is sometimes missed in the literature where a same slope is often used both for the direct and inverse method in the Cepheid calibration even as these slopes differ from the slopes that apply to the cluster data).

In the preceding sections we have used a variety of slopes, some arbitrary and others calculated from the Cepheid data, and some from the composite cluster with various magnitude truncations. Table 7 summarizes all of the choices discussed in the previous sections.

The equations of the regressions in Table 7 are $M = a \log w_{20} + b$ and $B = a \log w_{20} + c$ where the a, b, and c values are listed in columns (1), (2), and (4) of the table. Column (3) is the rms of the absolute magnitude zero point calibration, b, in column (2). Column (5) is the rms of the apparent magnitude zero point in column (4). Column (6) identifies the sample used, ranging from $n = 92$ for the total sample, $n = 84$ for the total sample truncated at $B = 14.0$, to $n = 78$ for a sample still further truncated by eliminating the four outliers on the bight side and the two outliers on the faint side near the limit lines in Figures 5 and 6. Column (7) shows the mean distance modulus using the cluster data with the listed b and c calibrations and the magnitude limits for the cluster data in column (8). The moduli in column (7) are the differences between columns (4) and (2). The first five rows are the results for the run of assumed slopes discussed in § 6.1.

The strong dependence of the final moduli (summed to the cluster magnitude limit over the range of B from about 10 to 15 mag) on the slope of the TF regression is shown by the variation in column (7) for the slopes in first five rows of the table. For the more restricted range of the slopes shown by the four pairs of values in the last part of the table, the modulus values range from 31.30 to 31.60. The values for the highest weight sample (i.e. that with the lowest rms values) with $n = 78$, vary from $(m - M) = 31.42$ for the inverse solution to 31.56 for the direct solution.

It is of interest to set out the data for this highest weight sample in the same detail as in Table 5 for the complete sample. Table 8 lists the partial moduli in the various magnitude intervals and magnitude limits for the restricted sample format for the direct slope of -6.346 and the inverse slope of -7.519. Table 8A shows the results in magnitude intervals; Table 8B shows the results of summing to various magnitude limits.

The data are plotted in Figure 11. The open circles are from Table 8A; the crosses from Table 8B. The noise in the correlations is caused by the nonuniform filling of the correlation between $B = 12$ and 14, mentioned earlier.

7.2. The Adopted Distance Modulus for the Virgo A, Virgo B and Ursa Major I and II Clusters

From Table 8 and Figure 11 we adopt as our final TF modulus for the composite cluster the mean of the direct and inverse calculation using the $n = 78$ restricted sample. The values from Table 8B are $(m - M) = 31.56 \pm 0.05$ for the direct calculation and $(m - M) = 31.41 \pm 0.05$ for the inverse, giving $\langle m - M \rangle = 31.49 \pm 0.04$ as the weighted mean.

Following FTS 98 (§ 8 there) we apply a systematic correction of 0.07 mag (reducing

the modulus) to account for the fact that the cluster members at a given LW are redder on average (and also are hydrogen deficient) than for the calibrators. Hence, our final TF modulus of the Virgo A cluster is $(m - M) = 31.42 \pm 0.04$ (internal).

Applying the magnitude offset from Virgo A to Virgo B of 0.38 ± 0.16 mag (Virgo B is more distant than Virgo A), of 0.16 ± 0.13 mag for UMa I made closer, and 0.16 ± 0.17 mag for UMa II made further from § 4.1 gives the modulus values of these clusters as $(m - M) = 31.80 \pm 0.16$ for Virgo B, 31.26 ± 0.13 for UMa I, and 31.58 ± 0.17 for UMa II.

7.3. Systematic Errors

The formal (internal) error of ± 0.04 for Virgo A is, of course, too small because of systematic errors in (1) the Cepheid P-L relation of the order of 0.1 mag in its zero point (Tammann et al. 2007), and the error in the zero point of equations (5) and (6) here, (2) the uncertainty of ~ 0.1 mag in the zero point of the Cepheid TF regression in Figure 8 (cf. the Cepheid rms value in Table 7), and (3) the statistical noise due to the nonuniform filling of the TF correlation in Figures 5 and 6 as discussed above. It is impossible to put an exact value on the systematic accuracy of $(m - M)$ due to these causes, but a reasonable estimate is that it is no smaller or larger than ± 0.2 mag. Hence, we adopt $(m - M) = 31.42 \pm 0.2$ mag as our final modulus of Virgo A using the Tully-Fisher method.

If, as is sometimes done, we combine Virgo A and B, treating them as a single cluster with $(m - M) = 31.42 \pm 0.2$ (assumed) from 43 galaxies in Virgo A and $(m - M) = 31.80 \pm 0.2$ (assumed) from Virgo B from 16 galaxies, the weighted mean of A and B is $(m - M) = 31.52 \pm 0.14$ (external assumed), which, however, we do not use. For comparison, the value derived by FTS 98 (their eq. 11) where clusters A and B are combined, is 31.58 ± 0.24 (external).

7.4. The Hubble Constant from the Adopted Virgo A Distance

From the discussion by FTS 98 (Fig. 14 and § 11.2), the expansion velocity of the Virgo core, freed from all streaming motions and tied to the external cosmic frame beyond the local bubble whose edge is near $4000\,\mathrm{km\,s^{-1}}$ (Jerjen & Tammann 1993; FST 94, Figs. 17-19; Masters et al. 2006), is $1175\,\mathrm{km\,s^{-1}}$. This is derived from a high weight solution of the relative Hubble diagram (velocity vs. distance *ratios*) by Jerjen & Tammann (1993) where the Virgo core is tied to 17 more remote clusters augmented by 24 clusters from Giovanelli (private communication in 1996) who also used distance ratios to Virgo.

Taking Virgo A to be the core relative to which the distance ratios to the 41 galaxies pertains, and using $(m - M) = 31.42 \pm 0.2$ ($D = 19.2$ Mpc, with a range from 17.5 to 21.1 Mpc) combined with $1175\,\mathrm{km\,s^{-1}}$ for the free expansion velocity, the resulting Hubble constant is $H_0 = 61\,\mathrm{km\ \ s^{-1}\ \ Mpc^{-1}}$ with a range from 53 to 70, where we have also put an error of $\pm 50\,\mathrm{km\,s^{-1}}$ on the Virgo A expansion velocity.

If, for some reason, one does not wish to rely on the distance ratios to Virgo of Jerjen & Tammann (1993), as augmented by Giovanelli's private communication in 1996, another route to obtain the free expansion velocity of the Virgo core is via a velocity perturbation model for the Virgo velocity relative to the remote frame. The observed mean heliocentric velocity of the Virgo core is $1050 \pm 35\,\mathrm{km\,s^{-1}}$ (Binggeli et al. 1993). This transforms to $932\,\mathrm{km\,s^{-1}}$ relative to the centroid of the Local Group (Yahil, Tammann, & Sandage 1977). Using $v(\mathrm{infall}) = 220\,\mathrm{km\,s^{-1}}$ (Kraan-Korteweg 1986) for the Virgo infall velocity gives $v_{\mathrm{Virgo}} = 1152 \pm 35\,\mathrm{km\,s^{-1}}$ which is the same as $1175\,\mathrm{km\,s^{-1}}$ to within statistics.

The value of $H_0 = 61$ obtained here agrees well with the value determined via the supernovae route in 25 separate studies, most of which give H_0 between 50 and 70 (summarized in Table 6 of Sandage et al. 2006) by a plethora of authors. However, we consider the method here to be of considerably lower weight than that using supernovae because of the evident problems raised by the population incompleteness bias when using clusters and the problem of tying the Virgo A cluster accurately into the remote cosmic kinematic frame.

REFERENCES

Binggeli, B., Popescu, C. C., & Tammann, G. A. 1993, A&AS, 98, 275

Binggeli, B., Sandage, A., & Tammann, G. A. 1985, AJ, 90, 1681

Bottinelli, L., Chamaraux, P., Gérard, E., Gouguenheim, L., Heidmann, J., Kazès, I., & Lauqué, R. 1971, A&A, 12, 264

Bottinelli, L., Gouguenheim, L., Fouqué, P., Paturel, G., & Teerikorpi, P. 1987, A&A, 181, 1

Bottinelli, L., Gouguenheim, L., Paturel, G., & Teerikorpi, P. 1986, A&A, 156, 157

Bottinelli, L., Gouguenheim, L., Paturel, G., & Teerikorpi, P. 1988a, ApJ, 328, 4

Bottinelli, L., Gouguenheim, L., & Teerikorpi, P. 1988b, A&A, 196, 17

de Vaucouleurs, G. 1975, in Galaxies and the Universe, eds. A. Sandage, M. Sandage, & J. Kristian, Vol. 9 of Univ. Chicago Press Compendium, 557

de Vaucouleurs, G., de Vaucouleurs, A., Corwin, H. G., Buta, R. J., Paturel, G., & Fouqué, P. 1991, Third Catalogue of Bright Galaxies (New York: Springer) (RC3)

Ekholm, T., & Teerikorpi, P. 1997, A&A, 325, 33

Federspiel, M. 1999, PhD thesis, University Basel

Federspiel, M., Sandage, A., & Tammann, G. A. 1994, ApJ, 430, 29 (Paper III), (FST 94)

Federspiel, M., Tammann, G. A., & Sandage, A. 1998, ApJ, 495, 115 (FTS 98)

Feigelson, E. D., & Babu, G. J. 1992, ApJ, 397, 55

Fouqué, P., Bottinelli, L., Gouguenheim, L., & Paturel, G. 1990, ApJ, 349, 1

Freedman, W. L., et al. 2001, ApJ, 553, 47

Giovanelli, R., Haynes, M. P., Herter, T., Vogt, N. P., Wegner, G., Salzer, J. J., da Costa, L. N., & Freudling, W. 1997a, AJ, 113, 22

Giovanelli, R., et al. 1997b, AJ, 113, 53

Gouguenheim, L. 1969, A&A, 3, 281

Hendry, M. A., & Simmons, J. F. L. 1994, Vistas Astron., 39, 297

Humason, M. L., Mayall, N. U., & Sandage, A. R. 1956, AJ, 61, 97

Jerjen, H., & Tammann, G. A. 1993, A&A, 276, 1

Kanbur, S. M., & Ngeow, C. C. 2004, MNRAS, 350, 962

Kapteyn, J. C. 1914, ApJ, 40, 43

Kraan-Korteweg, R. C. 1986, A&AS, 66, 255

Kraan-Korteweg, R. C., Cameron, L. M., & Tammann, G. A. 1988, ApJ, 331, 620

Klypin, A., Hoffman, Y., Kravtsov, A. V., & Gottlöber, S. 2003, ApJ, 596, 19

Malmquist, K. G. 1920, Lund Medd. Ser. II, 22, 1

Malmquist, K. G. 1922, Lund Medd. Ser. I, 100, 1

Masters, K. L., Springob, C. M., Haynes, M. P., & Giovanelli, R. 2006, ApJ, 653, 861

Ngeow, C. C., & Kanbur, S. M. 2005, MNRAS, 360, 1033

Ngeow, C. C, Kanbur, S. M., Nikolaev, S., Buonaccorsi, J., Cook, K. H., & Welch, D. L. 2005, MNRAS, 363, 831

Peletier, R. F., & Willner, S. P. 1993, ApJ, 418, 626

Pierce, M. J., & Tully, R. B. 1988, ApJ, 330, 579

Roberts, M. S. 1969, AJ, 74, 859

Saha, A., Thim, F., Tammann, G. A., Reindl, B., & Sandage, A. 2006, ApJS, 165, 108

Sandage, A. 1988a, ApJ, 331, 583

Sandage, A. 1988b, ApJ, 331, 605

Sandage, A. 1994a, ApJ, 430, 1 (Paper I)

Sandage, A. 1994b, ApJ, 430, 13 (Paper II)

Sandage, A. 1999, AJ, 117, 157 (Paper VII)

Sandage, A., & Tammann, G. A. 1981, 1987, A Revised Shapley Ames Catalog of Bright Galaxies, Carnegie Pub. 635 (Washington: Carnegie Institution of Washington)

Sandage, A., Tammann, G. A., & Federspiel, M. 1995, ApJ, 452, 1 (Paper IV), (STF 95)

Sandage, A., Tammann, G. A., & Reindl, B. 2004, A&A, 424, 43

Sandage, A., Tammann, G. A., Saha, A., Reindl, B., Macchetto, F. D., & Panagia, N. 2006, ApJ, 653, 843

Schechter, P. L. 1980, AJ, 85, 801

Scott, E. L. 1957, AJ, 62, 248

Seares, F. H. 1944, ApJ, 100, 255

Sérsic, J. L. 1960, Zs. f. Ap, 50, 168

Tammann, G. A., Sandage, A., & Reindl B. 2003, A&A, 404, 423

Tammann, G. A., Sandage, A., & Reindl, B. 2007, ApJ, submitted

Teerikorpi, P. 1984, A&A, 141, 407

Teerikorpi, P. 1987, A&A, 173, 39

Teerikorpi, P. 1990, A&A, 234, 1

Teerikorpi, P. 1997, ARA&A, 35, 101

Teerikorpi, P., Ekholm, T., Hanski, M. O., & Theureau, G. 1999, A&A, 343, 713

Theureau, G., Hanski, M., Ekholm, T., Bottinelli, L., Gouguenheim, L., Paturel, G., & Teerikorpi, P. 1997a, A&A, 322, 730

Theureau, G., Hanski, M., Teerikorpi, P., Bottinelli, L., Ekholm, T., Gouguenheim, L., & Paturel, G. 1997b, A&A, 319, 435

Tully, R. B. 1988, Nature, 334, 209

Tully, R. B., & Fisher, J. R. 1977, A&A, 54, 661

Tully, R. B., & Fisher, J. R. 1987, Atlas of Nearby Galaxies (Cambridge: Cambridge Univ. Press)

Tully, R. B., Verheijen, M. A. W., Pierce, M. J., Huang, J.-S., & Wainscoat, R. J. 1996, AJ, 112, 2471

Verheijen, M. A. W. 1997, PhD thesis, University Groningen

Willick, J. A. 1994, ApJS, 92, 1

Yahil, A., Tammann, G. A., & Sandage, A. 1977, ApJ, 217, 903

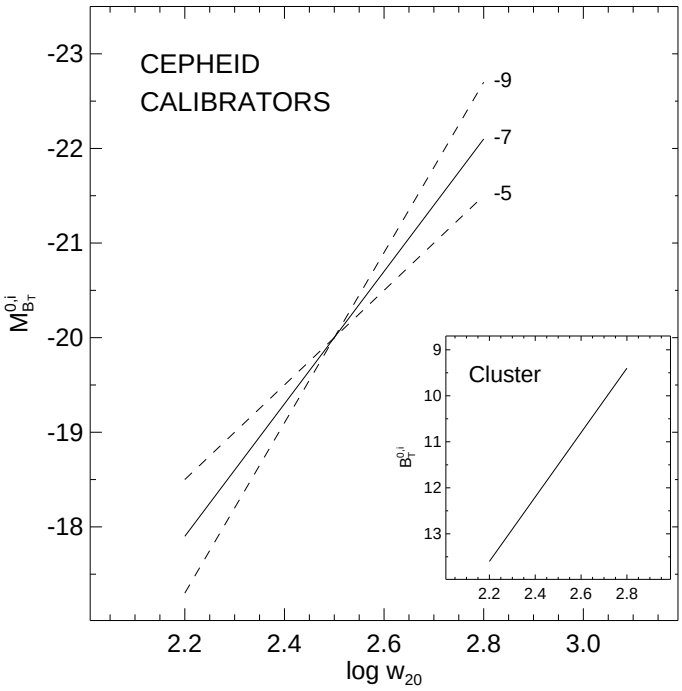

Fig. 1.— Model of a toy cluster (the insert) with a dispersionless TF correlation of line width (corrected for inclination) with apparent magnitude that has a slope of $dB_T^{0,i}/d\log w_{20} = -7$. A calibration of absolute magnitude with LW in the main body of the diagram is shown with variations in the TF slope ranging from -9 to -5.

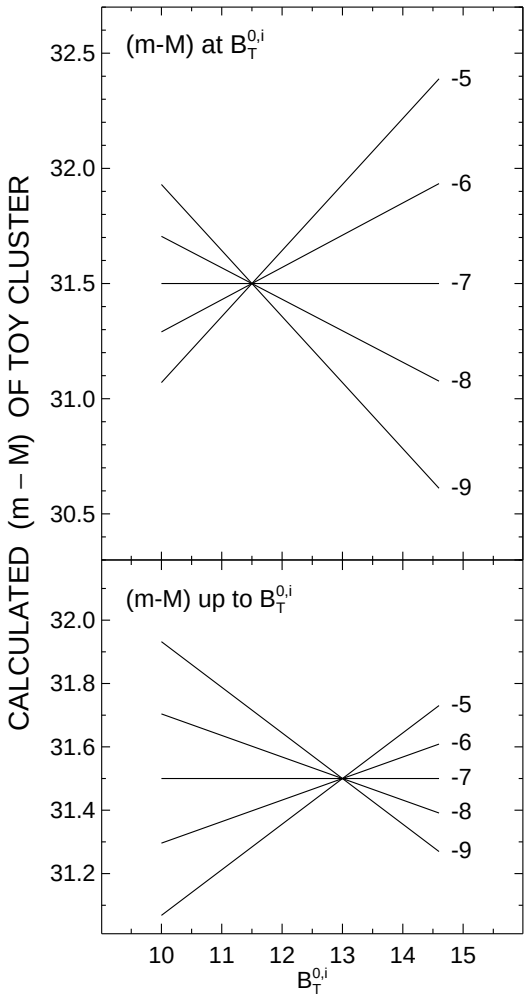

Fig. 2.— (top): The variation of the derived distance modulus *at* a given sampling magnitude into the cluster luminosity function for five assumed TF slope values from data in the first half of Table 1. All modulus values cross at $(m - M) = 31.5$ by construction. (bottom): The mean modulus summed to the listed cut-off magnitude for the five slope values from the second half of Table 1. The correct modulus of $(m - M) = 31.5$ is obtained only when $B_T^{0,i}$ stops at 13.0 for all slope values that differ from the true slope of -7. This magnitude is symmetrical about the cross-over magnitude of 11.5 (by construction). Sampling fainter than the symmetrical magnitude of 13.0 will give incorrect distance moduli, except for the case of the correct slope of -7.

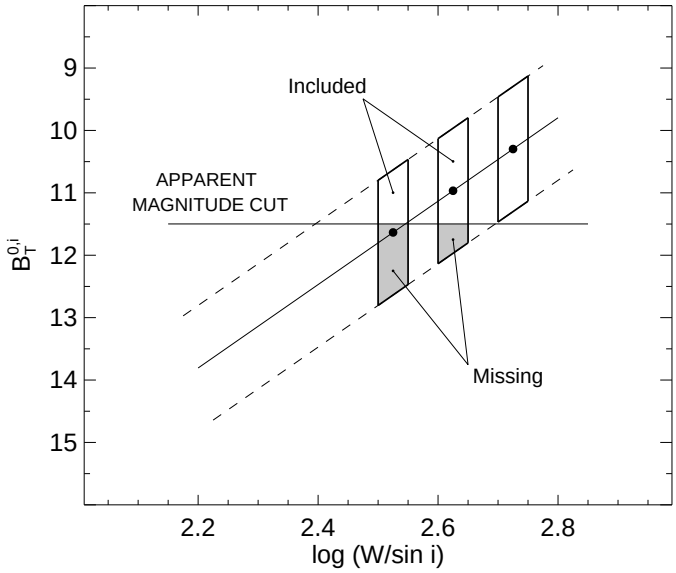

Fig. 3.— Model of the TF correlation in a cluster with intrinsic dispersion and/or an appreciable back-to-front ratio. The bias effect of an incomplete sampling of the cluster luminosity function is shown, given, for illustration, an observer's magnitude cut-off limit at $B_T^{0,i} = 11.5$. The right hand vertical LW interval is unbiased because none of the data in it are denied entrance into the sample fainter; all are brighter than the cut-off magnitude. However, the line width intervals to the left are progressively biased at this magnitude cut-off. The incompleteness bias at any given cut-off magnitude is found by summing over all line widths brighter than the cut-off value.

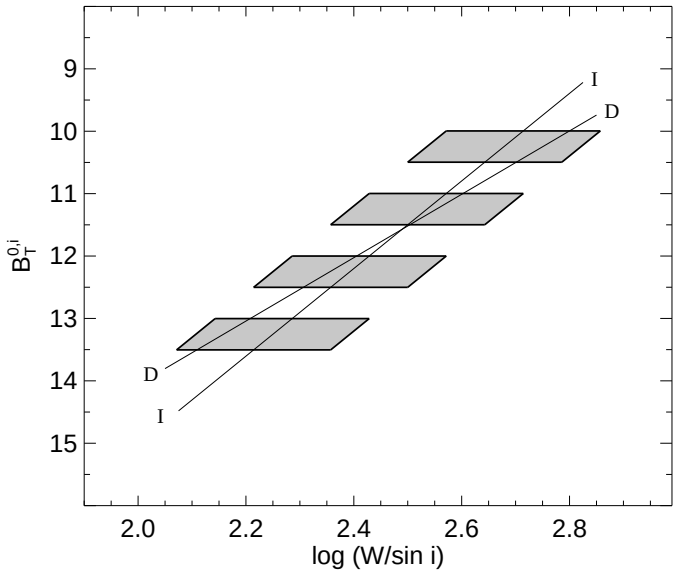

Fig. 4.— The data for a cluster are binned in apparent magnitude intervals. Four magnitude intervals are shown, each enclosed by envelope lines that show the intrinsic dispersion (and/or back-to-front effect) in LW at given apparent magnitudes. Slopes for both the direct and inverse TF least squares ridge lines for the calibrators are shown schematically.

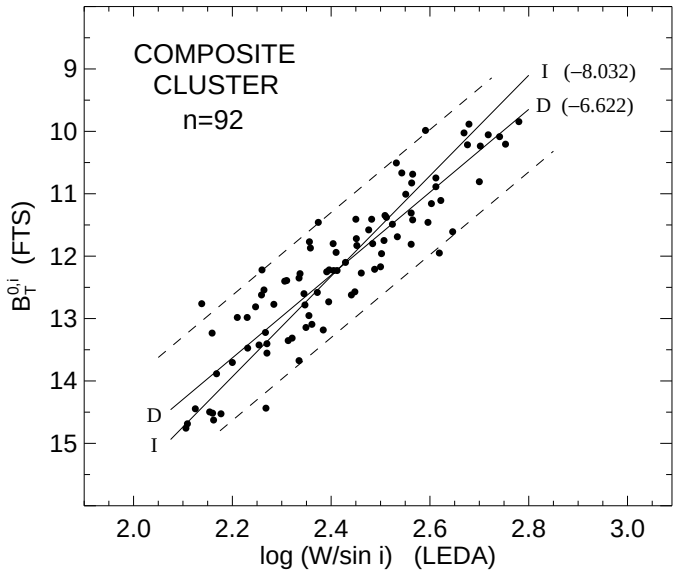

Fig. 5.— The correlation of line width, corrected for inclination, with apparent magnitude for the 92 galaxies in the composite cluster composed of galaxies from the Virgo A and B subclusters and the Ursa Major cloud as reduced to the distance of the Virgo A subcluster. The ridge lines for the direct and inverse least squares regressions are shown whose slopes are in parentheses. The dashed envelope lines are put one magnitude brighter and fainter than the direct ridge line. The magnitudes are on the FTS 98 system (their Table 3) which is within a few hundredths of a magnitude of the RC3 $B_T^{0,i}$ fully corrected system. The line widths are on the LEDA system which is 0.033 ± 0.002 dex smaller than the RC3 system. The equations of the ridge lines are equations (1) and (2) of the text.

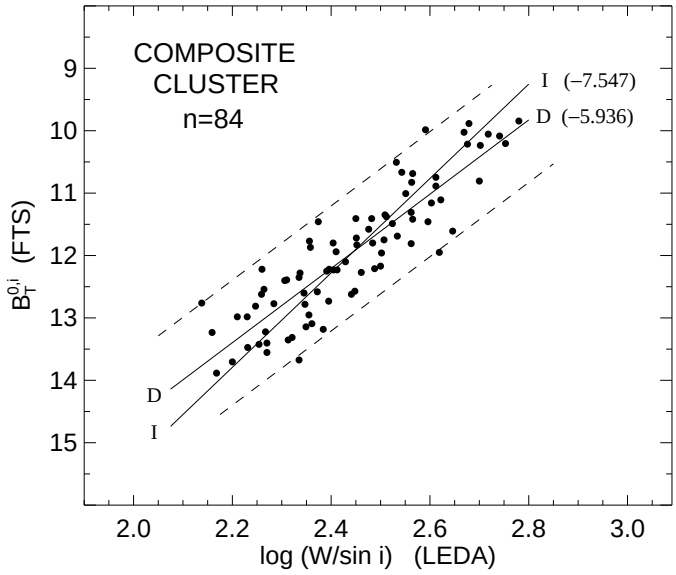

Fig. 6.— Same as Figure 5 but for a restricted sample of 84 galaxies in the artificial cluster, cut from the total sample by $B_T^{0,i} < 14.0$. The equations of the direct and inverse ridge lines are equations (3) and (4) of the text.

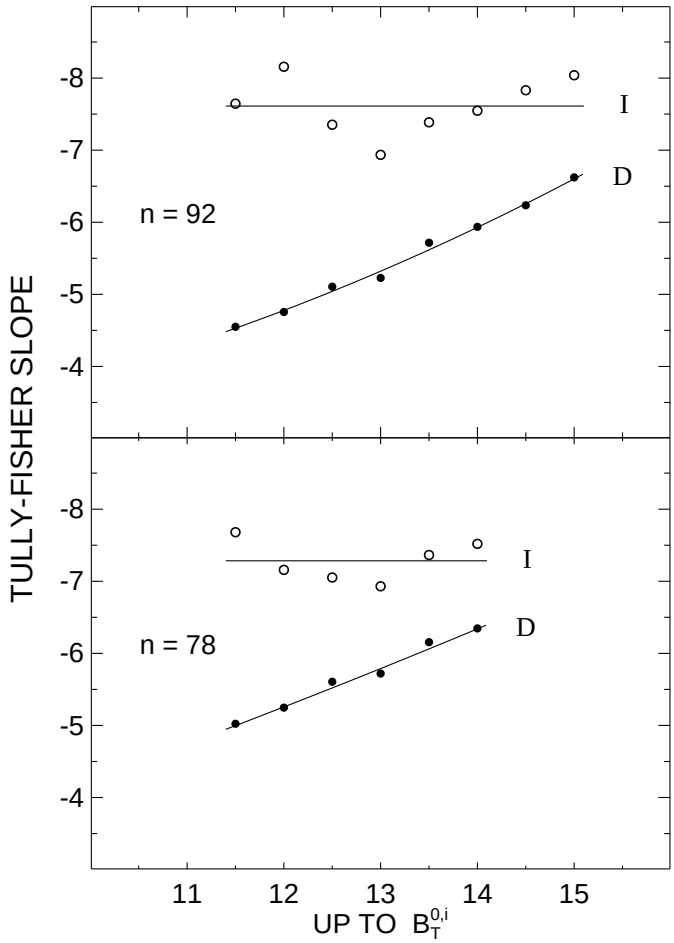

Fig. 7.— (Top) Change of the Tully-Fisher slope for partial samples as depth of penetration into the cluster luminosity function increases using data for the total ($n = 92$) sample. The DIRECT (dots) and INVERSE (open circles) least squares solutions are shown as the number of galaxies in the solutions increases from 28 to 92 and the magnitude cut-offs range from $B_T^{0,i} = 11.0$ to 15.0. (Bottom) Same for the restricted sample of 78 galaxies. The data are from Table 2.

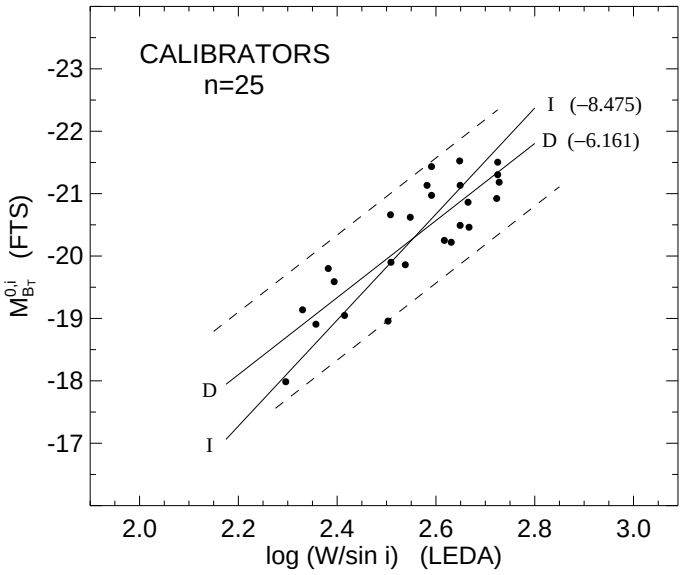

Fig. 8.— The Cepheid calibrator data from Table 3 shown with the least squares regressions for both the direct and inverse formulations whose slopes are in parentheses. These differ from the slopes from the data for the composite cluster in Figures 5 and 6, both of which have higher weight than the Cepheid sample alone.

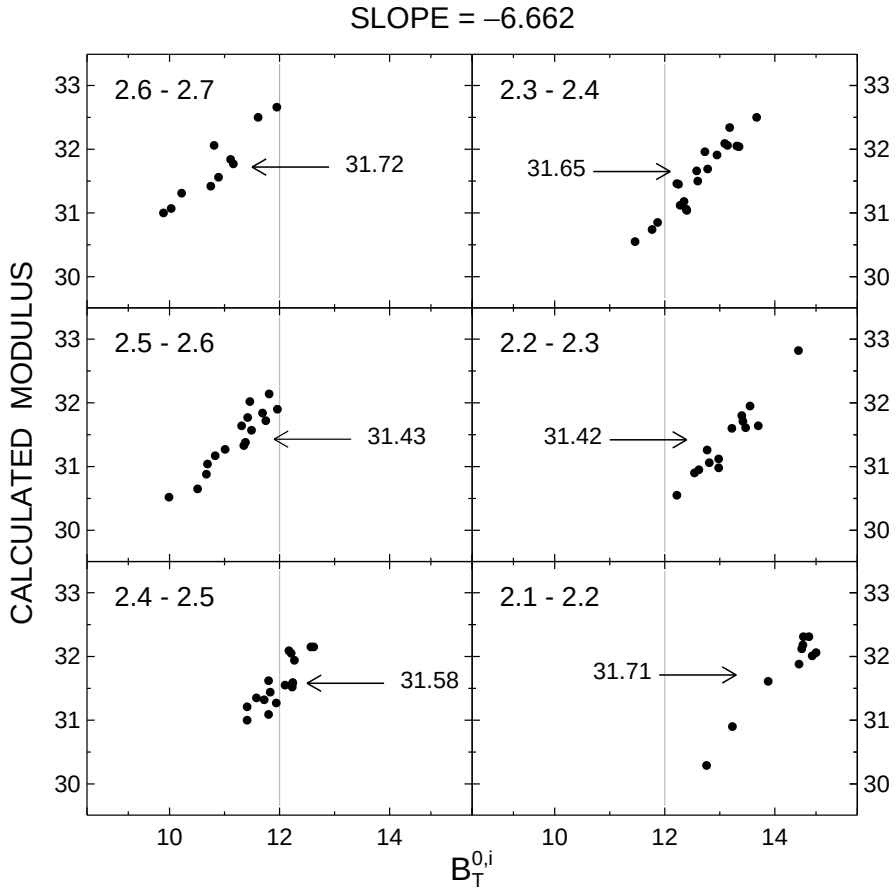

Fig. 9a.— The variation with apparent magnitude of the calculated distance moduli for each galaxy in the artificial cluster when binned in $\log w_{20}$ intervals in steps of 0.1 dex using the DIRECT slope of -6.622 in Table 4A for the complete sample of $n = 92$. The mean modulus marked by the arrow in each panel is that listed at the bottom of Table 4A. A light vertical line to guide the eye is put in each panel at $B = 12.0$.

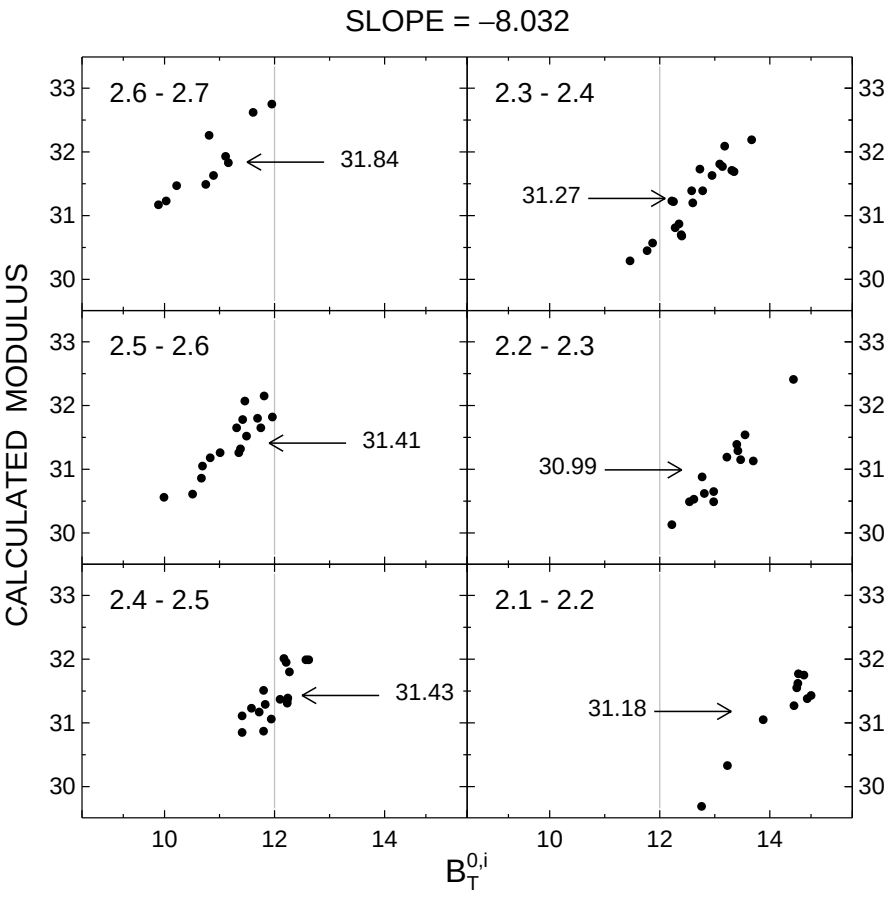

Fig. 9b.— Same as Figure 9a using the INVERSE slope of −8.032 and the individual data for the composite cluster.

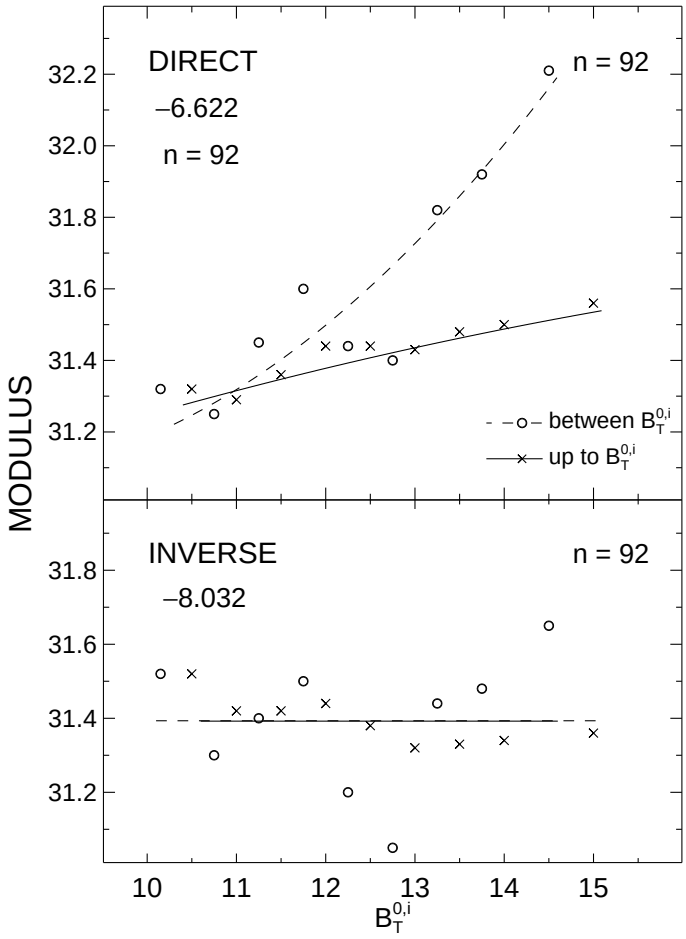

Fig. 10.— (Top). The average moduli for the total sample ($n = 92$) listed in Table 5 in each magnitude interval using the direct slope of -6.622 and summed over all line widths *in* that magnitude interval (open circles), and then summed over *all* magnitude intervals (crosses) up to the listed $B_T^{0,i}$ magnitude cut-off limit (crosses). (Bottom) Same for the inverse formulation with a slope of -8.032 for the total sample. The noise in both the open circle and the crosses data between $B = 12$ and 13 is caused by nonuniform filling of the TF distribution between the envelope lines of Figures 5 and 6. The data are from Table 5.

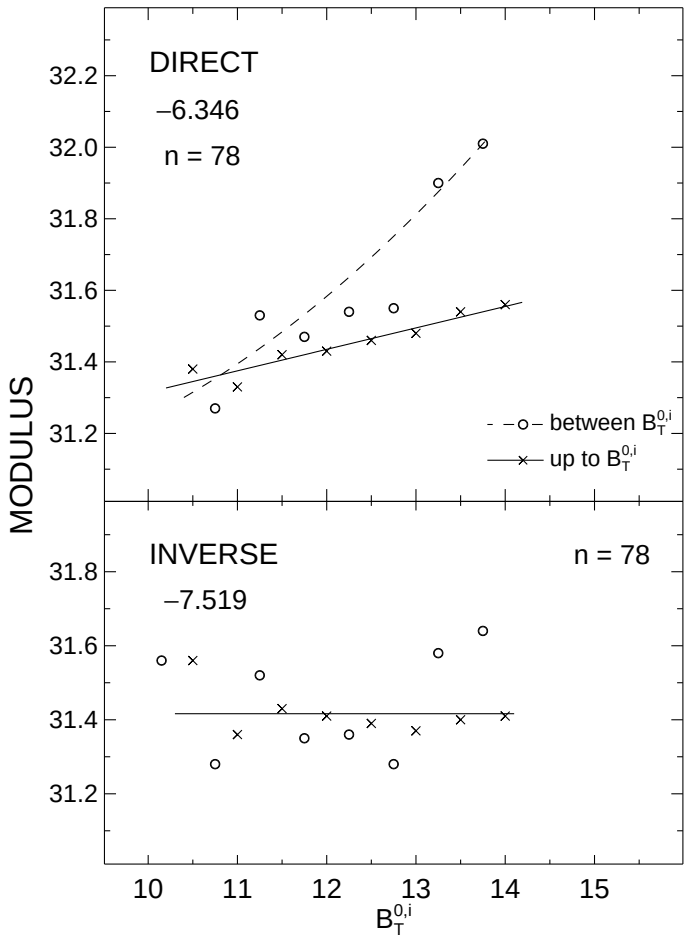

Fig. 11.— Similar to Figure 10 but for the restricted sample with $n = 78$. The Teerikorpi cluster population incompleteness bias is present using the direct TF slope but is absent using the inverse slope. The open circles are the modulus values from the data summed over all LW and averaged within the individual magnitude intervals (Table 8A). The crosses are the modulus values for the data summed aver all LW and then summed to the various magnitude cut-off limits (Table 8B).

Table 1. Derived Distance Moduli of the Toy Cluster of Figure 1 as a Function of $B_T^{0,i}$

	TF slope				
$B_T^{0,i}$	-9	-8	-7	-6	-5
(1)	(2)	(3)	(4)	(5)	(6)
	$(m-M)$ at $B_T^{0,i}$				
10.0	31.93	31.70	31.50	31.29	31.07
10.5	31.79	31.64	31.50	31.36	31.21
11.0	31.64	31.57	31.50	31.43	31.36
11.5	31.50	31.50	31.50	31.50	31.50
12.0	31.36	31.43	31.50	31.57	31.64
12.5	31.21	31.36	31.50	31.64	31.79
13.0	31.07	31.29	31.50	31.71	31.93
13.5	30.93	31.21	31.50	31.79	32.07
14.0	30.78	31.14	31.50	31.86	32.21
14.5	30.64	31.07	31.50	31.93	32.36
	$\langle m-M \rangle$ from data summed up to $B_T^{0,i}$				
10.0	31.93	31.70	31.50	31.29	31.07
10.5	31.86	31.67	31.50	31.33	31.14
11.0	31.79	31.64	31.50	31.36	31.21
11.5	31.72	31.60	31.50	31.40	31.28
12.0	31.64	31.57	31.50	31.43	31.36
12.5	31.57	31.53	31.50	31.47	31.43
13.0	31.50	31.50	31.50	31.50	31.50
13.5	31.43	31.46	31.50	31.54	31.57
14.0	31.36	31.43	31.50	31.57	31.64
14.5	31.28	31.39	31.50	31.61	31.71

Table 2. Least Squares TF Regressions to Various Magnitude Cut-offs for the Total ($n = 92$) and the Restricted ($n = 78$) Sample of the Composite Cluster

		Total DIRECT		Total INV			Restricted DIRECT	INV
$B_T^{0,i}$	n	Slope	Zpt	Slope	Zpt	n	slopes	
(1)	(2)	(3)	(4)	(5)	(6)	(7)	(8)	(9)
< 11.5	28	-4.550	22.603	-7.645	30.653	26	-5.023	-7.680
< 12.0	42	-4.755	23.290	-8.157	31.998	38	-5.247	-7.158
< 12.5	56	-5.106	24.251	-7.353	29.909	51	-5.606	-7.052
< 13.0	70	-5.228	24.610	-6.935	28.831	64	-5.720	-6.930
< 13.5	80	-5.716	25.888	-7.386	29.983	74	-6.155	-7.364
< 14.0	84	-5.936	26.454	-7.547	30.391	78	-6.346	-7.519
< 14.5	87	-6.235	27.216	-7.831	31.101	...	...	...
< 15.0	92	-6.622	28.195	-8.032	31.603	...	...	...

Table 3. The Cepheid Calibrators

Name	Type	$(m-M)$ Saha 06	$B_T^{0,i}$ FTS 98	$M_{B(T)}^{0,i}$ FTS 98	$\log w_{20}$
(1)	(2)	(3)	(4)	(5)	(6)
NGC 224	SbI-II	24.54	3.36	−21.18	2.728
NGC 300	ScII.8	26.48	8.49	−17.99	2.296
NGC 598	Sc(s)II-III	24.64	5.73	−18.91	2.357
NGC 925	SBc(s)II-III	29.84	10.04	−19.80	2.382
NGC 1365	SBbc(s)I	31.46	9.94	−21.52	2.648
NGC 1425	Sb(r)II	31.96	10.83	−21.13	2.582
NGC 2090	Sc(s)II	30.48	11.52	−18.96	2.503
NGC 2403	Sc(s)III	27.43	8.38	−19.05	2.415
NGC 2541	Sc(s)III	30.50	11.36	−19.14	2.330
NGC 3031	Sb(r)I-II	27.80	7.34	−20.46	2.667
NGC 3198	Sc(s)I-II	30.80	10.14	−20.66	2.508
NGC 3319	SB(s)II.4	30.74	11.15	−19.59	2.394
NGC 3351	SBb(r)II	30.10	10.24	−19.86	2.538
NGC 3368	Sab(s)II	30.34	9.85	−20.49	2.649
NGC 3621	Sc(s)II.8	29.30	9.40	−19.90	2.509
NGC 3627	Sb(s)II.2	30.50	9.07	−21.43	2.591
NGC 4258	Sb(s)II	29.50	8.31	−21.13	2.649
NGC 4321	Sc(s)I	31.18	9.88	−21.30	2.725
NGC 4535	SBc(s)I.3	31.25	10.28	−20.97	2.591
NGC 4536	Sbc(s)I-II	31.24	10.62	−20.62	2.548
NGC 4548	SBb(rs)I-II	30.99	10.77	−20.22	2.631
NGC 4639	SB(r)II	32.20	11.95	−20.25	2.617
NGC 4725	Sb/SBb(r)II	30.65	9.73	−20.92	2.723
NGC 5457	Sc(s)I	29.17	8.31	−20.86	2.665
NGC 7331	Sb(rs)I-II	30.89	9.39	−21.50	2.725

Table 4. $\langle m - M \rangle$ Averaged within Various Discrete Intervals of Line Width and Listed in Magnitude Intervals for the Composite Cluster

	Log Line Width Intervals (w_{20})						
$B_T^{0,i}$	2.7-2.8	2.6-2.7	2.5-2.6	2.4-2.5	2.3-2.4	2.2-2.3	2.1-2.2
(1)	(2)	(3)	(4)	(5)	(6)	(7)	(8)
(A) DIRECT SLOPE = −6.622							
9.8-10.5	31.60 (5)	31.13 (3)	30.52 (1)				
10.5-11.0		31.68 (3)	30.94 (4)				
11.0-11.5		31.80 (2)	30.57 (7)	31.10 (2)	30.55 (1)		
11.5-12.0		32.58 (2)	31.90 (4)	31.35 (6)	30.79 (2)		
12.0-12.5				31.76 (7)	31.22 (6)	30.55 (1)	
12.5-13.0				32.15 (2)	31.74 (5)	31.05 (6)	30.29 (9)
13.0-13.5					32.12 (5)	31.68 (4)	30.90 (1)
13.5-14.0					32.50 (1)	31.79 (2)	31.61 (1)
14.0-15.0						32.82 (1)	32.12 (7)
Summed							
vertical	31.60	31.72	31.43	31.58	31.65	31.42	31.77
n	5	10	16	17	20	14	10
rms	0.145	0.563	0.483	0.372	0.556	0.573	0.667
(B) INVERSE SLOPE = −8.032							
9.8-10.5	31.85 (5)	31.29 (3)	30.56 (1)				
10.5-11.0		31.79 (3)	30.93 (4)				
11.0-11.5		31.88 (2)	31.32 (7)	30.98 (2)	30.29 (1)		
11.5-12.0		32.68 (2)	31.86 (4)	31.36 (6)	30.51 (2)		
12.0-12.5				31.60 (6)	30.13 (1)		
12.5-13.0				31.99 (2)	31.47 (5)	30.61 (6)	29.69 (1)
13.0-13.5					31.84 (5)	31.26 (4)	30.33 (1)
13.5-14.0					32.19 (1)	31.34 (2)	31.05 (1)
14.0-15.0						32.41 (1)	31.54 (7)
Summed							
vertical	31.85	31.84	31.41	31.43	31.27	30.99	31.18
n	5	10	16	17	20	14	10
rms	0.179	0.552	0.481	0.389	0.561	0.580	0.673

Table 5. $\langle m - M \rangle$ as Summed over all Line Widths for Various Magnitude Intervals and Cut-off Magnitudes for the Composite Cluster

between $B_T^{0,i}$	n	summed over LW $\langle m-M \rangle$	rms	up to $B_T^{0,i}$	n	summed over LW $\langle m-M \rangle$	rms
(1)	(2)	(3)	(4)	(5)	(6)	(7)	(8)
(A) DIRECT SLOPE = −6.622							
9.8-10.5	9	31.32	0.398	10.5	9	31.32	0.398
10.5-11.0	7	31.25	0.470	11.0	16	31.29	0.417
11.0-11.5	12	31.45	0.410	11.5	28	31.36	0.414
11.5-12.0	14	31.60	0.570	12.0	42	31.44	0.479
12.0-12.5	14	31.44	0.427	12.5	56	31.44	0.463
12.5-13.0	14	31.40	0.550	13.0	70	31.43	0.478
13.0-13.5	10	31.82	0.402	13.5	80	31.48	0.484
13.5-14.0	4	31.92	0.413	14.0	84	31.50	0.488
14.0-15.0	8	32.21	0.286	15.0	92	31.56	0.514
(B) INVERSE SLOPE = −8.032							
9.8-10.5	9	31.52	0.475	10.5	9	31.52	0.475
10.5-11.0	7	31.30	0.550	11.0	16	31.42	0.504
11.0-11.5	12	31.40	0.510	11.5	28	31.42	0.495
11.5-12.0	14	31.50	0.693	12.0	42	31.44	0.561
12.0-12.5	14	31.20	0.527	12.5	56	31.38	0.558
12.5-13.0	14	31.05	0.676	13.0	70	31.32	0.594
13.0-13.5	10	31.44	0.495	13.5	80	31.33	0.581
13.5-14.0	4	31.48	0.300	14.0	84	31.34	0.576
14.0-15.0	8	31.65	0.354	15.0	92	31.36	0.566

Table 6. $\langle m - M \rangle$ as Summed to Various Magnitude Cut-offs over all LW for Different Tully-Fisher Slopes

Summed to		SLOPES							
		−9		−7		−6		−5	
$B_T^{0,i}$	n	$\langle m - M \rangle$	rms	$\langle m - M \rangle$	rms	$\langle m - M \rangle$	rms	$\langle m - M \rangle$	rms
(1)	(2)	(3)	(4)	(5)	(6)	(7)	(8)	(9)	(10)
10.5	9	31.66	.524	31.37	.418	31.23	.365	31.09	.317
11.0	16	31.51	.567	31.33	.439	31.23	.383	31.14	.339
11.5	28	31.45	.563	31.37	.433	31.33	.388	31.29	.366
12.0	42	31.44	.632	31.44	.498	31.44	.455	31.44	.436
12.5	56	31.34	.643	31.43	.485	31.46	.437	31.50	.423
13.0	70	31.23	.697	31.40	.504	31.48	.447	31.56	.434
13.5	80	31.23	.678	31.44	.504	31.55	.467	31.65	.497
14.0	84	31.22	.671	31.46	.505	31.57	.477	31.69	.497
15.0	92	31.23	.651	31.51	.518	31.65	.525	31.78	.576

Table 7. Regressions for the Cepheid Calibration and for the Composite Cluster for Various Tully-Fisher Slopes: the Sensitivity of the Resulting Distance Moduli to Slope

Slope	Cepheid calib.[5)]		Cluster[6)]		n	$\langle m-M \rangle$	$B_T^{0,i}$
a	b	rms	c	rms		to sample end	
(1)	(2)	(3)	(4)	(5)	(6)	(7)	(8)
−9	+2.716	0.624	33.946	0.651	92	31.23	15.0
−8	+0.197	0.541	31.525	0.564	92	31.33	15.0
−7	−2.402	0.511	29.108	0.518	92	31.51	15.0
−6	−4.961	0.499	26.689	0.525	92	31.65	15.0
−5	−7.519	0.522	24.261	0.576	92	31.78	15.0
−6.161[1)]	−4.549	0.500	27.078	0.520	92	31.63	15.0
−8.475[1)]	+1.364	0.580	32.664	0.598	92	31.30	15.0
−6.622[2)]	−3.369	0.502	28.191	0.514	92	31.56	15.0
−8.032[2)]	+0.239	0.557	31.609	0.566	92	31.37	15.0
−5.936[3)]	−5.124	0.500	26.456	0.477	84	31.58	14.0
−7.547[3)]	−1.003	0.533	30.387	0.538	84	31.39	14.0
−6.346[4)]	−4.077	0.499	27.483	0.415	78	31.56	14.0
−7.519[4)]	−1.077	0.530	30.343	0.451	78	31.42	14.0

[1)]Cepheid least squares regressions, n = 25

[2)]Direct and inverse slopes for total cluster sample (Fig. 5)

[3)]Direct and inverse slopes for cluster sample cut at $B_T^{0,i} = 14.0$ (Fig. 6)

[4)]Direct and inverse slopes for final sample (with a $B = 14.0$ cut plus six others eliminated)

[5)]Cepheid calibration as $M_{B(T)} = a \log w_{20} + b$

[6)]Cluster regression as $B_T^{0,i} = a \log w_{20} + c$

Table 8. Modulus of the Composite Cluster for Various Magnitude Intervals and Limits from the High Weight Restricted Sample

Interval $B_T^{0,i}$	n	Slope= −6.346 Direct (78) $\langle m-M\rangle$	rms	Slope= −7.519 Inverse (78) $\langle m-M\rangle$	rms
(1)	(2)	(3)	(4)	(5)	(6)
(A) IN MAGNITUDE INTERVALS					
9.8-10.5	8	31.78	.270	31.56	.311
10.5-11.0	7	31.27	.505	31.28	.521
11.0-11.5	11	31.53	.299	31.52	.355
11.5-12.0	12	31.47	.407	31.35	.482
12.0-12.5	13	31.54	.339	31.36	.412
12.5-13.0	13	31.55	.446	31.28	.535
13.0-13.5	10	31.90	.383	31.58	.461
13.5-14.0	4	32.01	.396	31.64	.480
(B) TO MAGNITUDE CUT-OFF LIMITS					
10.5	8	31.38	.270	31.56	.311
11.0	15	31.33	.386	31.36	.442
11.5	26	31.42	.360	31.43	.407
12.0	38	31.43	.371	31.41	.427
12.5	51	31.46	.363	31.39	.420
13.0	64	31.48	.379	31.37	.444
13.5	74	31.54	.404	31.40	.449
14.0	78	31.56	.415	31.41	.451